

Investigation of Austenite-to-Ferrite Transformation in Ultralow and Low-Carbon Steel Using High-Speed Quenching Dilatometry and Thermokinetic Simulation



F. IMTIAZ and E. KOZESCHNIK

The isothermal austenite decomposition kinetics is studied in 0.004 wt pct C ultralow carbon (ULC) and 0.11 wt pct C low-carbon (LC) steel using high-speed quenching dilatometry. Standard samples of these steels are heated to austenitization temperatures of 1223 K and 1373 K (950 °C and 1100 °C) and then quenched to testing temperatures between 1163 K and 933 K (890 °C and 660 °C). The measured and calculated austenite-to-ferrite phase fractions are compared with dilatation values to analyze the ferrite nucleation and growth conditions during austenite decomposition. Ferrite evolution profiles are assessed to investigate the underlying growth kinetics. The analysis in ULC steel shows regimes of partitionless, partitioning, and two-stage transformation kinetics. In contrast, LC steel shows only diffusion-controlled transformation kinetics. The experimental results are well reproduced with thermokinetic calculations, thus supporting our interpretation of governing mechanisms during transformation.

DOI: 10.1007/s11661-017-4078-x

© The Minerals, Metals & Materials Society and ASM International 2017

I. INTRODUCTION

THE decomposition of austenite can give birth to a variety of industrially important morphologies such as ferrite, bainite, and martensite. Therefore, the kinetics of austenite decomposition is of immediate relevance to the metal processing industry. The kinetics is dependent on the phase transformation mechanisms, which play a pivotal role in microstructure-forming processes that tune these morphologies. The austenite (γ)–to–ferrite (α) transformation is one of the most complex of these processes.

Commonly, long-range diffusion-controlled as well as martensitic and massive transformation mechanisms are operative in steels. Long-range diffusion-controlled transformation occurs at low cooling rates, because these rates allow for equilibrium partitioning of (interstitial) alloying elements, such as carbon (C), during phase separation. Bhadeshia^[1] and Christian^[2] characterize the austenite-to-ferrite transformation as a part of reconstructive transformation mechanisms. Martensitic transformations occur at high cooling rates, because substantial diffusion during phase separation is practically suppressed. Experimentally, these high cooling rates are obtained by rapidly quenching the austenite to

room temperature. At intermediate cooling rates, either the massive or the two-stage transformation mechanism is operative. The massive transformation also does not involve any partitioning of alloying elements. The product phase (α) inherits the chemical composition of the parent phase (γ) and is characterized by a microstructure with the typical appearance of “massive grains.” In the two-stage transformation observed in the present work, phase separation proceeds in two stages. Either the first stage can proceed without partitioning or vice versa, depending on the cooling rates.

Massalski^[3] investigated the massive transformations in iron and its alloys at intermediate cooling rates, *i.e.*, at cooling rates high enough to avoid long-range diffusion-controlled transformations and, at the same time, not high enough to allow for martensitic transformations. Bibby and Parr^[4] studied the effect of cooling rate on the mechanism of austenite-to-ferrite transformation in ultralow carbon (ULC) steel using a gas quench unit with supersonic gas velocities for obtaining cooling rates in excess of 35,000 K/s. They plotted the transformation start temperature as a function of cooling rate and observed that the trend follows a two-plateau behavior. The plateau, which was obtained at medium cooling rates up to 5000 K/s and higher transformation start temperature, was attributed to the massive transformation of ferrite, whereas the reaction observed at lower transformation start temperature and higher cooling rates in excess of 35,000 K/s was attributed to the martensitic transformation. In similar materials, Kozeschnik and Gamsjäger^[5] and Liu *et al.*^[6,7] reported a two-stage transformation mechanism at cooling rates smaller than 700 K/s using dilatometry.

F. IMTIAZ is with the Institute of Materials Science and Technology, TU Wien, 1060 Wien, Austria, and also with Materials Division, Directorate of Technology, PINSTECH, Islamabad 45650, Pakistan. E. KOZESCHNIK is with the Institute of Materials Science and Technology, TU Wien. Contact e-mail: farhan_92saifi@yahoo.com

Manuscript submitted September 22, 2016.

Article published online April 6, 2017

In the present work, we (1) improve the quenching rates compared to the previous analysis using a high-speed quenching dilatometer, but we also (2) apply an alternative and more general thermokinetic approach (MatCalc) to interpret the experimental results. For the investigation of the austenite-to-ferrite transformation in ULC and low-carbon (LC) steels, cooling rates of 900 to 3400 K/s are obtained with thin-walled hollow cylindrical samples along with optimized He-jet valve opening times. Simultaneously, for comparison, the same study is also carried out for solid cylindrical samples of LC and ULC steel at constant 40 K/s.

The measured dilatation profiles exhibit, typical massive, two-stage and diffusion-controlled transformation characteristics.^[8] In order to assess the ferrite nucleation and growth conditions, measured and calculated onset temperatures and their corresponding dilatation are compared. The dilatation profiles are used for calculation of ferrite fraction evolution profiles. Thermodynamic and kinetic calculations are performed for ortho-equilibrium (OE), para-equilibrium (PE), or massive nucleation conditions. In addition, phase transformation simulations based on different growth models are carried out and compared to the measured transformed ferrite fractions to aid in interpretation of the experimental results.

II. EXPERIMENTAL

The chemical composition of the ULC and LC steels of industrial quality used in the present study in the as-received condition is shown in Table I. The chemical composition is obtained by spark erosion optical spectroscopy. The experiments are performed in a BÄHR (805A) high-speed quenching dilatometer (BÄHR Thermodynamics, Hüllhorst, Germany). The size of the samples conforms to the standard dimensions suggested in the specifications for dilatometric investigations^[9] (Figure 1). The heat treatment cycle is shown in Figure 2.

The specimens are heated at a rate of 100 K/s to austenitization temperatures (T_{aus}) of 1223 K and 1373 K (950 °C and 1100 °C), and soaked for 300 seconds at 1223 K (950 °C) and 600 seconds at 1373 K (1100 °C) with the purpose of varying the austenite grain size before testing. They are then quenched in a He-jet to their isothermal (IT) annealing temperatures. In the hollow samples, an inward hole of approximately 3.6 mm is drilled to reduce the wall thickness and to increase the quenching speed. In the dilatometer, the conventional top surface He-jet is equipped with an additional nozzle, spraying He also onto the interior walls and quenching them simultaneously with the outer

surface. The experiments are performed according to standard A 1033-04^[10] with temperature undershoots smaller than 20 K and stable thermal profiles within a time period of 2 seconds after reaching the IT annealing temperatures.

For the solid cylindrical samples, maximum cooling rates of approximately 40 K/s are obtained. In the case of hollow cylindrical samples, maximum cooling rates between 900 and 3400 K/s are achieved in the dilatometer by applying the maximum He pressure possible with the equipment and by optimizing the opening time of the fully opened valve to reach the IT temperature. The corresponding values and the measured cooling rates are summarized in Table II.

Previous work of Kozeschnik and Gamsjäger^[5] showed that austenite decomposition, in their experiments and with similar quenching rates, can start in the quenching segment before reaching the IT annealing temperatures. Consequently, any thermal undershoots, if present, would have significant influence on the evaluation of the onset of austenite-to-ferrite transformation, which is why we carefully control the valve opening times to avoid this effect. For solid samples of alloys A and B and hollow samples of alloy B, the IT annealing temperatures are reached without considerable undershoots and overshoots. The amounts of undershoots and overshoots observed in the case of thermal profiles of hollow samples of alloy A are shown in Table III. The values of these undershoots and overshoots are within the criteria set by the ASTM standard.

In order to avoid possible effects of unwanted plastic deformation during testing, the dilatometer push rods are adjusted in such a way that they exert the minimum force necessary to hold the samples securely between them. Other uncontrolled effects are avoided by only using fresh samples and by not reusing samples in repeated testing sequences.

After holding for sufficient time at IT annealing temperature to let the austenite-to-ferrite transformation complete, the specimens are quenched to room temperature. The representative microstructures of both alloys after performing the experiment are shown in Figure 3.

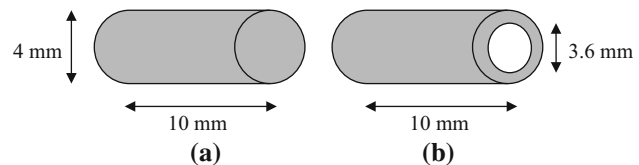


Fig. 1—Standard dimensions of (a) solid cylindrical and (b) hollow cylindrical samples.

Table I. Chemical Composition of Alloys A and B

Type of Steel	Alloy	Fe (Wt Pct)	C (Wt Pct)	Mn (Wt Pct)	Si (Wt Pct)
ULC	A	99.93	0.004	0.06	0.006
LC	B	98.79	0.11	0.93	0.17

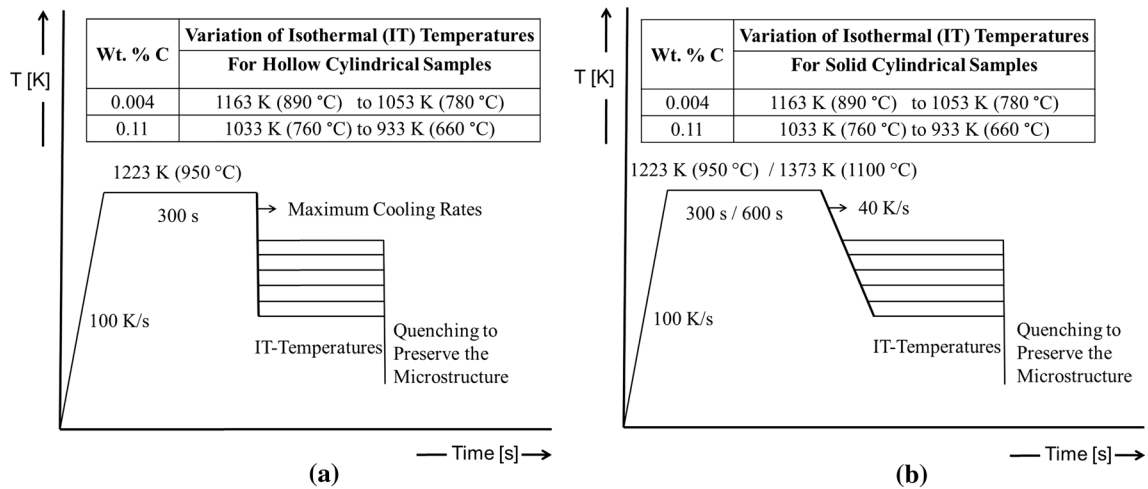


Fig. 2—Heat treatment cycles used for (a) hollow cylindrical and (b) solid cylindrical samples.

Table II. Optimized Valve Opening Times to Reach the IT Temperatures and the Maximal Cooling Rates for the Hollow Cylindrical Samples of Alloys A and B

Alloy	IT Temperature [K (°C)] $T_{\text{aus}} = 1223 (950)$	Optimized Valve Opening Time (ms)	Obtained Cooling Rates (K/s)
A	1163 (890)	18	900
	1153 (880)	20	1000
	1143 (870)	26	1850
	1133 (860)	25	1500
	1123 (850)	31	2700
	1053 (780)	50	3400
B	1033 (760)	56	2500
	993 (720)	71	2600
	933 (660)	83	3000

Table III. Values of Undershoots and Overshoots Observed in the Thermal Profile of Hollow Samples of Alloy A

Alloy	IT Temperature [K (°C)]	Undershoot (K)	Overshoot (K)
A	1163 (890)	2.0	2.0
	1153 (880)	1.0	2.5
	1143 (870)	2.9	2.9
	1133 (860)	2.3	6.4
	1123 (850)	5.1	11.0
	1053 (780)	0.0	25.0

III. RESULTS AND THERMODYNAMIC EQUILIBRIUM ANALYSIS

Experimentally measured thermal and dilatation profiles for hollow and solid cylindrical samples of alloys A and B with an austenitization temperature of 1223 K (950 °C) are shown in Figures 4 and 5. The profiles for solid samples of alloys A and B with an austenitization temperature of 1373 K (1100 °C) are shown in Figure 6. Only those segments of the thermal and dilatation profile associated with the quenching and austenite-to-ferrite transformation after soaking at austenitization temperature are displayed. During quenching, contraction and then expansion of the samples is observed. Contraction corresponds to the dilatational response of the sample to the quenching process, while

the apparent expansion is due to the volume change in the course of the austenite-to-ferrite transformation.

To compensate for the effect of the residual thermal undershoots and overshoots that remain even after optimization of the valve opening times, a rather pragmatic approach is used by comparing the measured and calculated dilatation profiles. The calculated dilatation profiles are obtained with the MatCalc software package,^[11,12] based on equilibrium thermodynamic evaluation and using the density data of ferrite and austenite as stored in the corresponding databases.^[13–15] These profiles are shown in Figure 7.

For the determination of measured onset temperatures and dilatations, the method suggested in Reference 5 is adopted. The measured dilatations are obtained

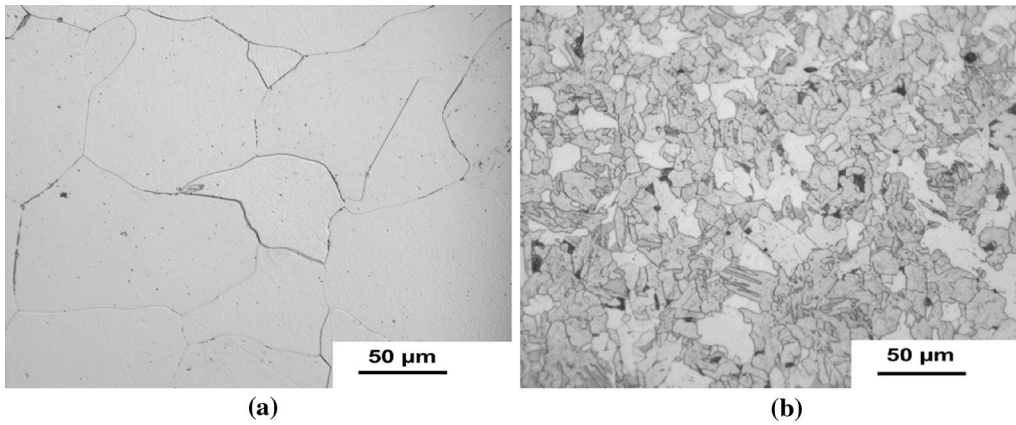


Fig. 3—Representative microstructures of (a) alloy A and (b) alloy B after testing.

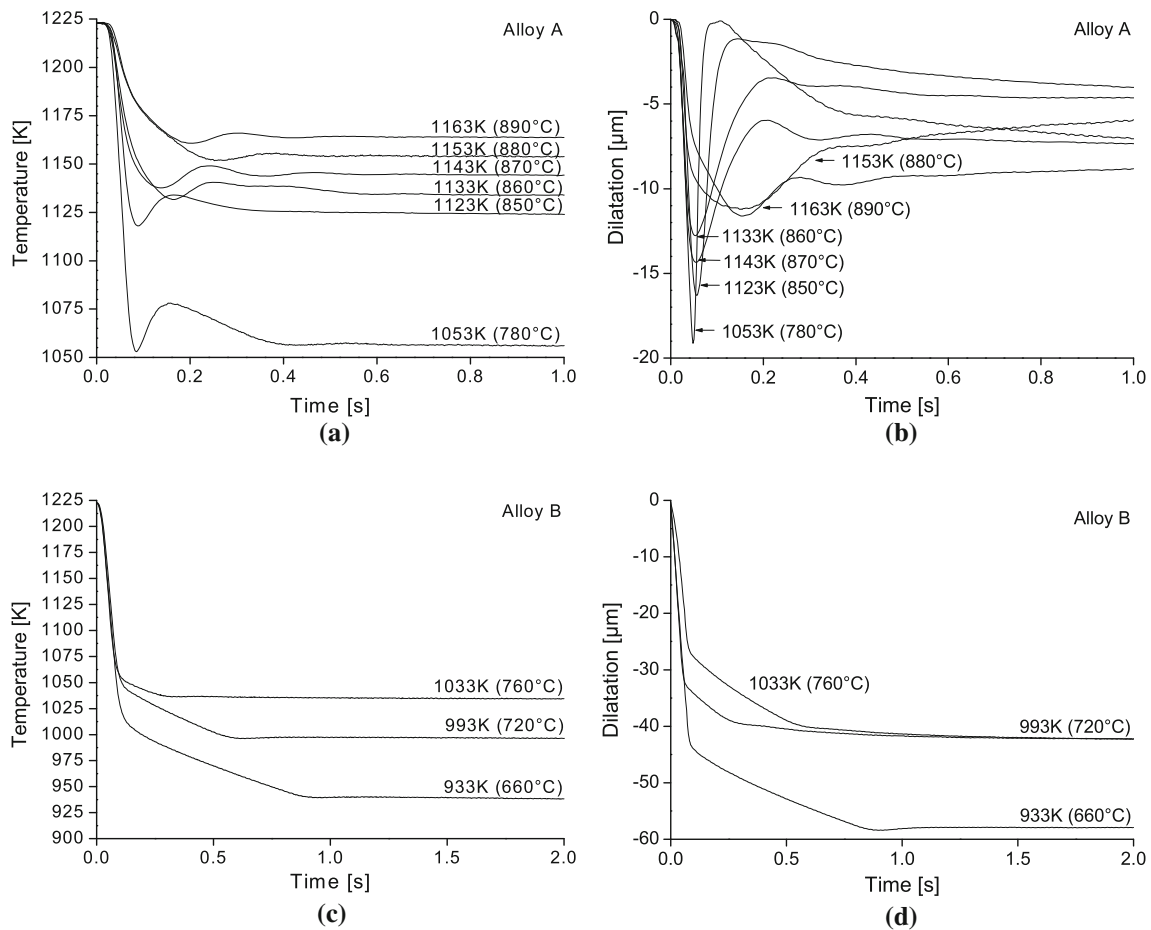


Fig. 4—Measured temperature and dilatation profiles for hollow samples of (a) and (b) alloy A and (c) and (d) alloy B obtained after austenitization at 1223 K (950 °C) for 300 s.

from the contraction part of the time vs dilatation (Figures 4(b), 5(b), and 6(b)) profiles and compared to the calculated temperature vs dilatation (Figure 7) profiles to determine the corrected onset temperature. The dilatation obtained for an IT temperature of 1123 K (850 °C), for instance, from the contraction part of the measured dilatation profiles, is $-13.5 \mu\text{m}$. Comparison of this contraction with the calculated

dilatation profile gives an onset temperature (T_{ons}) of 1164 K (891 °C). The measured contractions and their corresponding onset temperatures for alloy A are summarized in Table IV.

For the computational analysis of the austenite-to-ferrite onset temperatures and their corresponding dilatations, three possible scenarios are considered (e.g., References 1 through 3 and 16 through 21).

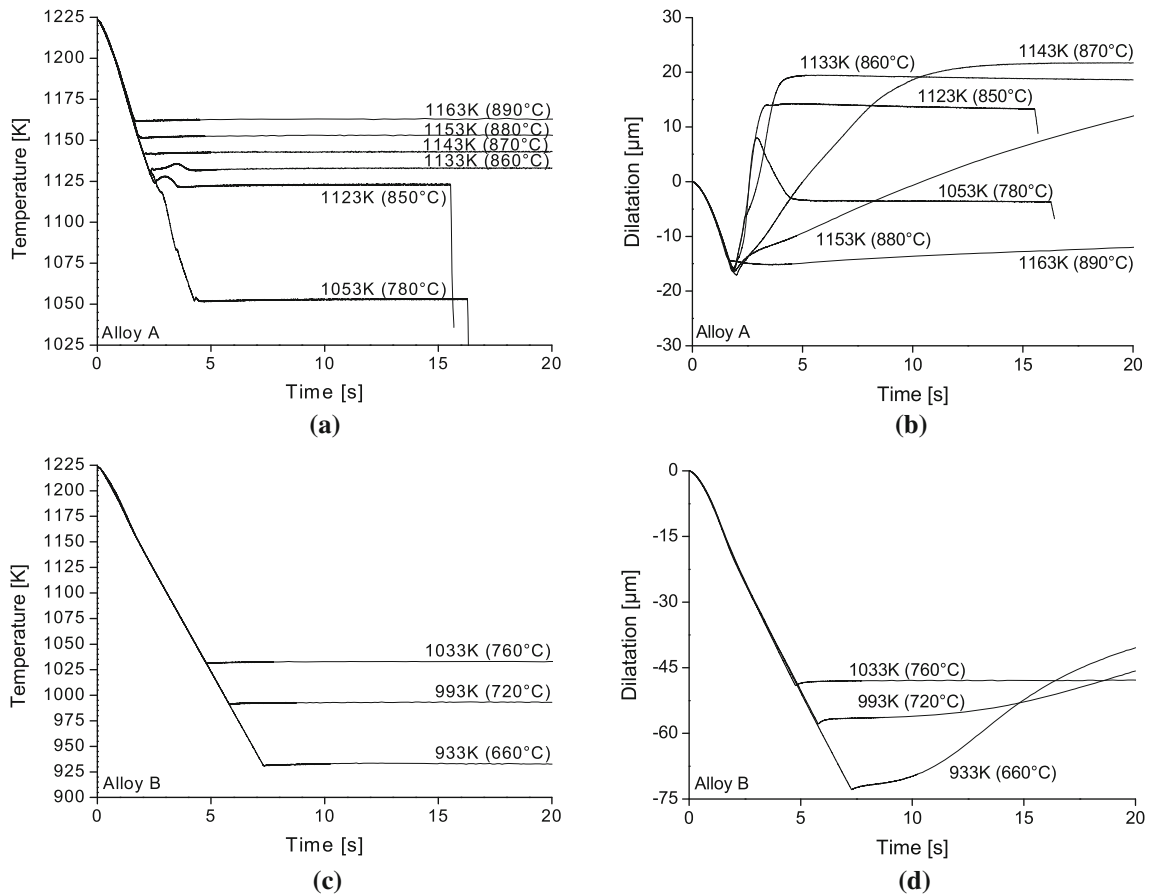


Fig. 5—Measured temperature and dilatation profiles for solid samples of (a) and (b) alloy A and (c) and (d) alloy B obtained after austenitization at 1223 K (950 °C) for 300 s.

- (1) OE transformation, *i.e.*, all alloying elements (C, Mn, and Si) partition between austenite and ferrite during transformation.
- (2) PE transformation, *i.e.*, partitioning of only interstitial C is possible between austenite and ferrite during transformation.
- (3) Massive transformation, *i.e.*, the T_o temperature defines the threshold for the austenite-to-ferrite transformation without redistribution of either interstitial (*i.e.*, C) or substitutional (*i.e.*, Mn and Si) alloying elements during transformation. The product phase (ferrite) inherits the chemical composition of the parent (austenite) phase.

The kinetics of transformation in the first two cases is slow, because redistribution (partitioning) of alloying elements requires time. The third case is characterized by fast transformation kinetics, because it does not involve any long-range diffusion of C or other alloying elements.

The calculated OE, PE, and massive phase boundaries and their corresponding dilatations (from Figure 7) for the austenite-to-ferrite transformation are summarized in Table V. The corresponding phase diagrams of alloys A and B are shown in Figures 8 and 9, respectively.

When investigating the required dilatation below the austenitization temperature that corresponds to a

certain equilibrium transformation temperature, we identify a contraction of $-10.1 \mu\text{m}$ (Table V) as the minimum dilatation necessary before nucleation of ferrite with equilibrium chemical composition can theoretically take place for alloy A. A minimum dilatation of $-11 \mu\text{m}$ (Table V) is required before nucleation of ferrite in the massive mode can commence.

All dilatation profiles, for hollow samples as well as for solid cylindrical samples, of alloy A and with an austenitization temperature of 1223 K (950 °C) show contractions exceeding $11 \mu\text{m}$ and an onset temperature lower than 1175.4 K (902.4 °C). Similarly, the solid cylindrical samples with austenitization at 1373 K (1100 °C) also show more contraction than is required for the equilibrium nucleation of ferrite. The onset temperature was lower than 1175 K (902 °C) in all cases. The onset temperature for hollow samples, as shown in Table IV, does not decrease significantly with increasing undercooling, which is an indication of the massive nature of transformation. These results are in line with the results of Kozeschnik and Gamsjäger.^[5]

For alloy B, in all cases, the onset of ferrite formation occurs after reaching the IT temperatures. The required driving force for OE, PE, and massive conditions is shown in Figure 10. At all IT temperatures down to 1033 K (760 °C), the driving force for massive

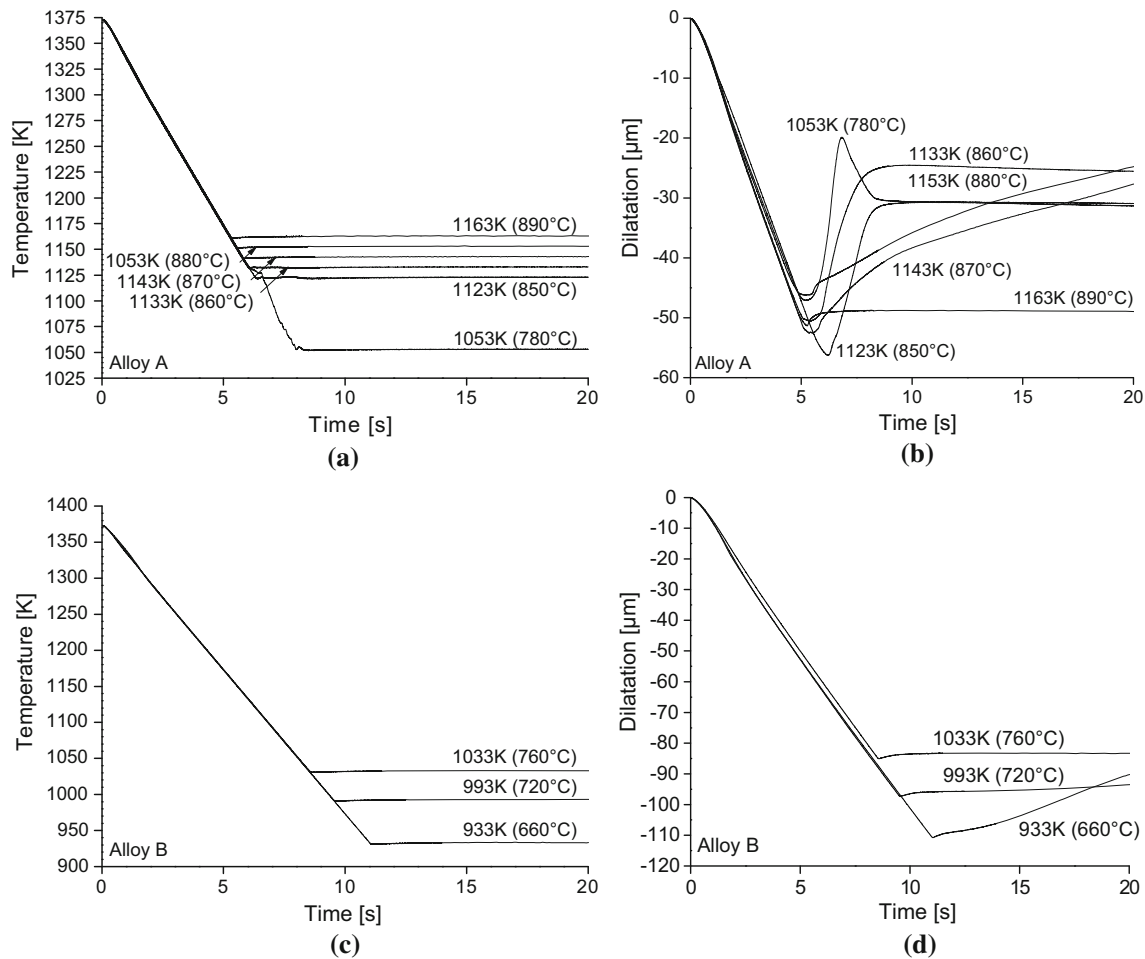


Fig. 6—Measured temperature and dilatation profiles for solid samples of (a) and (b) alloy A and (c) and (d) alloy B obtained after austenitization at 1373 K (1100 °C) for 600 s.

nucleation is negative, which suggests that the transformation must occur under C partitioning. The dilatation profiles obtained at IT temperatures of 993 K (720 °C) and 933 K (660 °C) show more contraction than required for massive nucleation. For example, a contraction of 44.2 μm would be required at an austenitization temperature of 1223 K (950 °C), and 78.7 μm is required for 1373 K (1100 °C). We conclude that the massive nucleation of newly formed ferrite is suppressed due to the necessity of partitioning of C also at these temperatures. At 993 K (720 °C), the driving force available for massive nucleation is almost 97 J/mol. At this temperature, the onset of ferrite formation appears sluggish, thus indicating a diffusion-controlled transformation mechanism. This applies also for an IT temperature of 933 K (660 °C), where the driving force for massive nucleation is 315 J/mol. These issues are further investigated later by computational phase transformation studies.

IV. THERMOKINETIC ANALYSIS

For further analysis of the transformation mechanism responsible for austenite decomposition, the dilatation

profiles are converted to ferrite fraction profiles. For convenience, the sample response from quenching, after austenitization, to completion of austenite-to-ferrite transformation is taken as threshold for zero and full transformation. Temperature transients after completion of the transformation are not displayed. The corresponding dilatation profiles of hollow samples of alloy A are corrected according to the procedure described previously. The corresponding curves are shown in Figures 11 and 12.

For the thermokinetic simulations, the precipitation kinetics module of the MatCalc software package^[11,12] is used. This software uses a fully predictive framework for the description of the nucleation kinetics based on classical nucleation theory and a general approach for calculating the interfacial energies. Nucleation of ferrite is assumed to occur at grain boundary corners.^[1–5] In addition to the calculation of effective interfacial energies according to the Generalized Broken Bond concept,^[22–24] we take into account the removal of prior austenite grain boundary area according to the Clemm and Fisher treatment.^[25] In our simulations, we observe that the ferrite/austenite interfacial energies observed under these conditions are extremely small and typically on the order of 26.5 mJ/m² for alloy A and 29.5 mJ/m²

for alloy B. As a consequence, nucleation can occur easily and with almost no undercooling.

Due to the difficulty of measuring the prior austenite grain size in this type of material, we assumed it to be

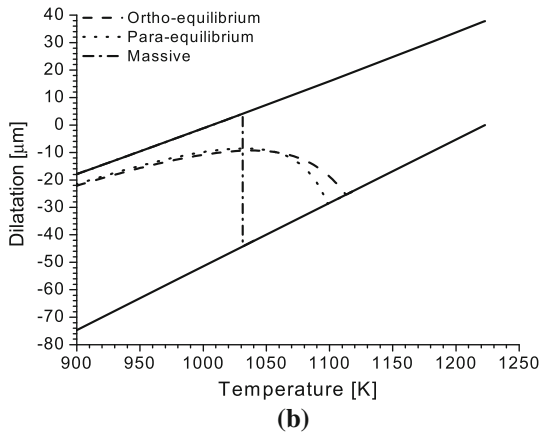
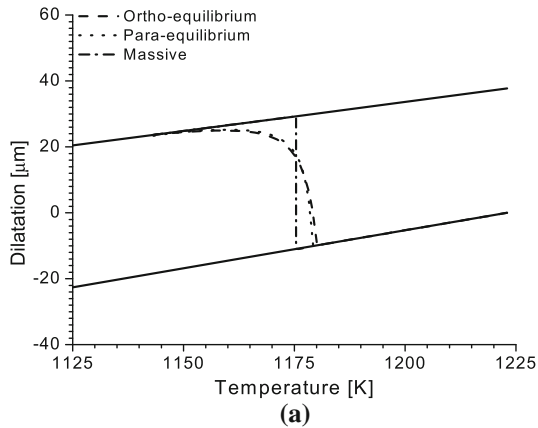


Fig. 7—Calculated equilibrium dilatation profiles of (a) alloy A and (b) alloy B starting at an austenitization temperature of 1223 K (950 °C) for the three transformation conditions considered in the present work.

equal to the resulting ferrite grain size at least for alloy A. This assumption is supported by additional experiments that were performed in a cyclic temperature profile, where we used the same sample for repeated austenite decomposition experiments. The results of

Table V. Calculated OE, PE, and Massive Austenite-to-Ferrite Phase Boundaries (T) and Their Corresponding Dilatations (ΔL) for Alloys A and B

Alloy	T [K (°C)]	ΔL (μm) $T_{\text{aus}} = 1223 \text{ K (950 } ^\circ\text{C)}$
A	1180.2 (907.2), OE	-9.9
	1179.2 (906.2), PE	-10.1
	1175.4 (902.4), massive	-11.0
B	1112.8 (839.8), OE	-25.4
	1098.4 (825.4), PE	-28.7
	1031.3 (758.3), massive	-44.2

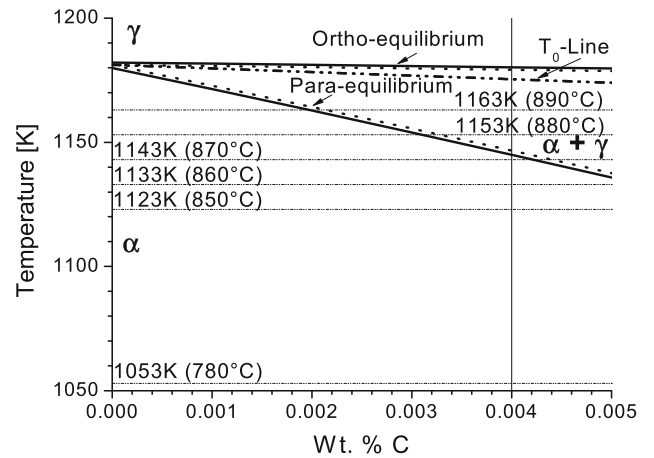


Fig. 8—Calculated equilibrium phase diagrams in OE and PE conditions for alloy A.

Table IV. Onset of the Austenite-to-Ferrite Transformations (T_{ons}) and Their Corresponding Dilatations in Alloy A

Alloy A	T_{aus} [K (°C)]	Target IT [K (°C)]	ΔL (μm)	T_{ons} [K (°C)]
Hollow samples	1223 (950)	1163 (890)	-11.6	1173 (900)
		1153 (880)	-11.2	1174 (901)
		1143 (870)	-12.1	1170 (897)
		1133 (860)	-11.8	1172 (899)
		1123 (850)	-13.5	1164 (891)
		1053 (780)	-18.0	1145 (872)
Solid samples	1223 (950)	1163 (890)	-13.8	1163 (890)
		1153 (880)	-16.2	1153 (880)
		1143 (870)	-15.5	1156 (883)
		1133 (860)	-15.4	1156 (883)
		1123 (850)	-15.4	1156 (883)
		1053 (780)	-15.4	1156 (883)
Solid samples	1373 (1100)	1163 (890)	-48.3	1163 (890)
		1153 (880)	-46.2	1172 (899)
		1143 (870)	-51.7	1148 (875)
		1133 (860)	-49.4	1158 (885)
		1123 (850)	-51.5	1149 (876)
		1053 (780)	-47.1	1168 (895)

these experiments show that the ferrite grain size is identical in all repeated tests, thus suggesting that the prior austenite grain size is stationary in the course of the cyclic tests from the first experiment on. The ferrite

grain size measured with the software ImageJ^[26] is 59 μm . The original austenite grain size in alloy B remains undetermined, because repeated testing shows continuously decreasing ferrite grain sizes and, thus, nonstationary prior austenite grain sizes.

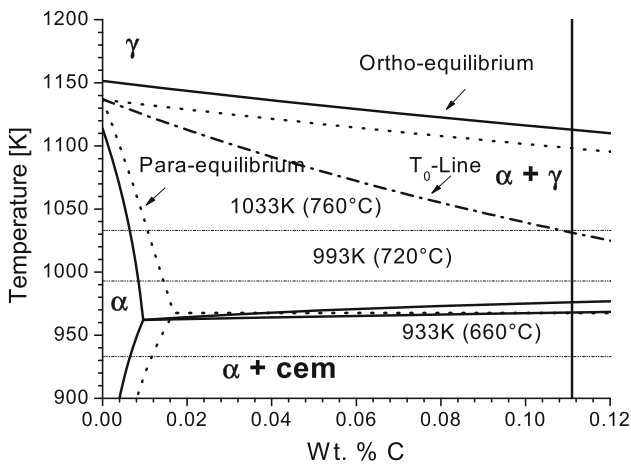


Fig. 9—Calculated equilibrium phase diagrams in OE and PE conditions for alloy B.

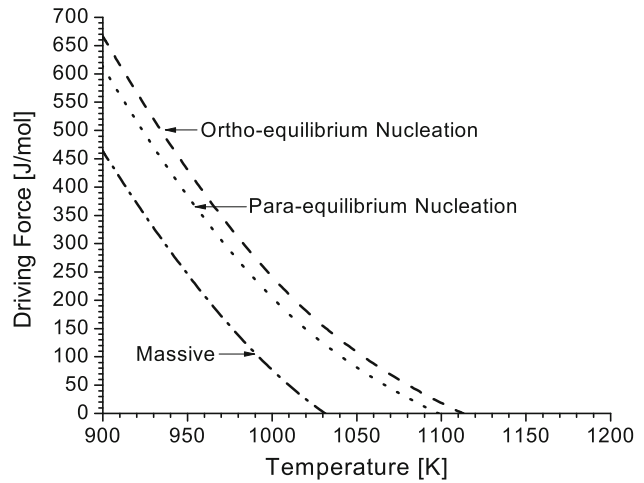


Fig. 10—Chemical driving force for nucleation in alloy B, calculated in OE, PE, and for massive nucleation conditions.

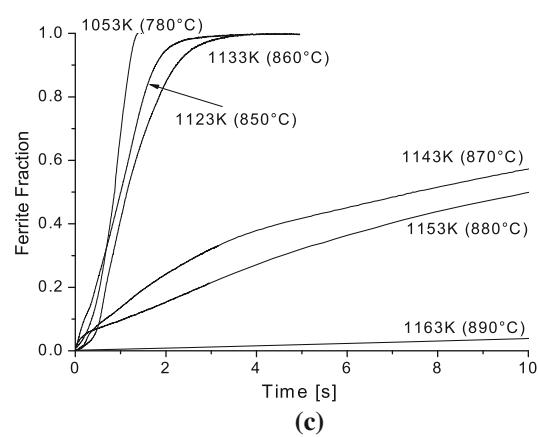
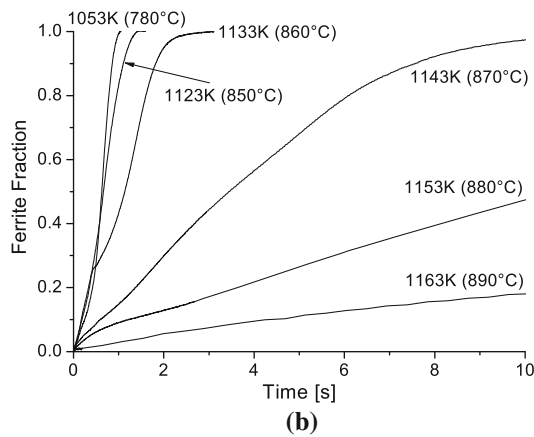
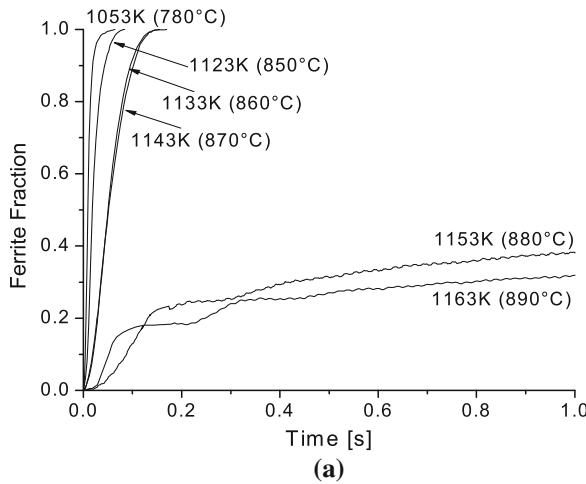


Fig. 11—Ferrite fraction evolution profiles of alloy A for (a) hollow samples with T_{aus} of 1223 K (950 °C), (b) solid samples with T_{aus} of 1223 K (950 °C), and (c) solid samples with T_{aus} of 1373 K (1100 °C).

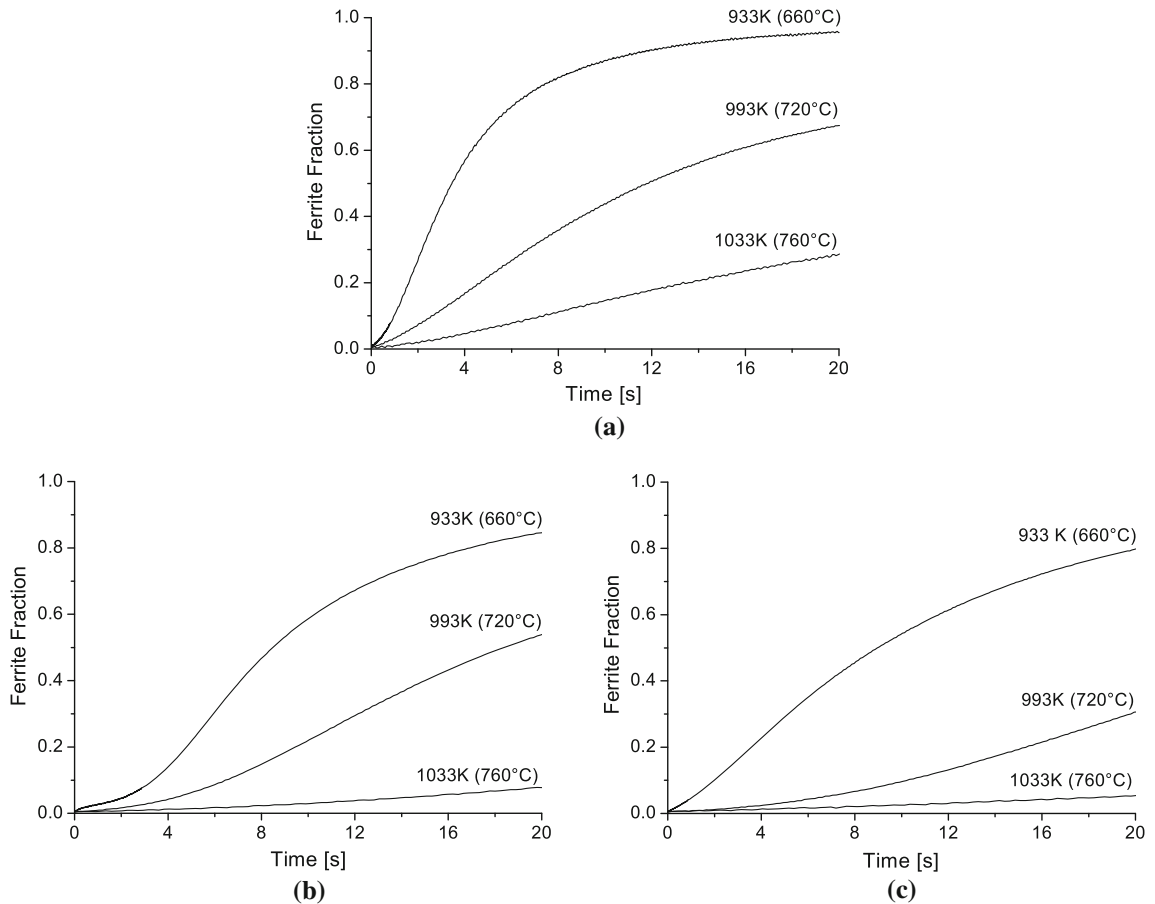


Fig. 12—Ferrite fraction evolution profiles of alloy B for (a) hollow samples with T_{aus} of 1223 K (950 °C), (b) solid samples with T_{aus} of 1223 K (950 °C), and (c) solid samples with T_{aus} of 1373 K (1100 °C).

A. Alloy A

1. Hollow samples

Figure 11(a) shows that the austenite decomposition kinetics in the hollow samples of alloy A in the ferrite single-phase region [IT temperatures between 1143 K and 1053 K (870 °C and 780 °C)] shows rapid transformation kinetics; *i.e.*, the transformation finishes in less than 100 ms. In all these samples, the transformation starts during quenching and the reaction rates cannot be suppressed even at the highest quenching rates achieved in the experiments. We conclude that such a fast transformation is only possible if it occurs without long-range partitioning of C or any other alloying element.

For substantiation of this statement, measured and simulated diffusion-controlled and partitionless kinetics for a sample quenched from 1223 K (950 °C) to the IT temperature of 1053 K (780 °C) is shown in Figure 13. Figures 13(b, c) clearly show that the calculated diffusion-controlled kinetics (in PE condition) is not consistent with the measured transformed ferrite fraction kinetics. For the diffusion-controlled case, the Svoboda–Fischer–Fratzl–Kozeschnik model,^[11,27] as implemented in the MatCalc package and the MatCalc mobility database,^[28] is used.

In contrast, the calculated partitionless transformation kinetics reproduces the measured ferrite fraction profile rather accurately. For the partitionless transformation, the same model is used as in the diffusion-controlled case, however, with the velocity of the phase boundary solely controlled by the intrinsic mobility of the austenite/ferrite interface, expressed as

$$M = M_0 \exp\left(-\frac{Q}{RT}\right) \quad [1]$$

In the present analysis, M_0 is taken as 5×10^{-4} mol s kg⁻¹ m⁻¹ and the value of activation energy, Q , as 140 kJ mol⁻¹.^[29,30] The calculations are performed for a ferrite grain size of 32 μm (Figure 13(c)).

In the two-phase region (Figure 11(a)), from IT temperatures of 1153 K and 1163 K (880 °C and 890 °C), the results indicate a two-stage transformation mechanism, where the control of reaction kinetics shifts from fast (massive) to relatively slower (long-range C-diffusion-controlled) kinetics. These results are in accordance with the previous experiments performed by Kozeschnik and Gamsjäger^[5] in the two-phase austenite-plus-ferrite region.

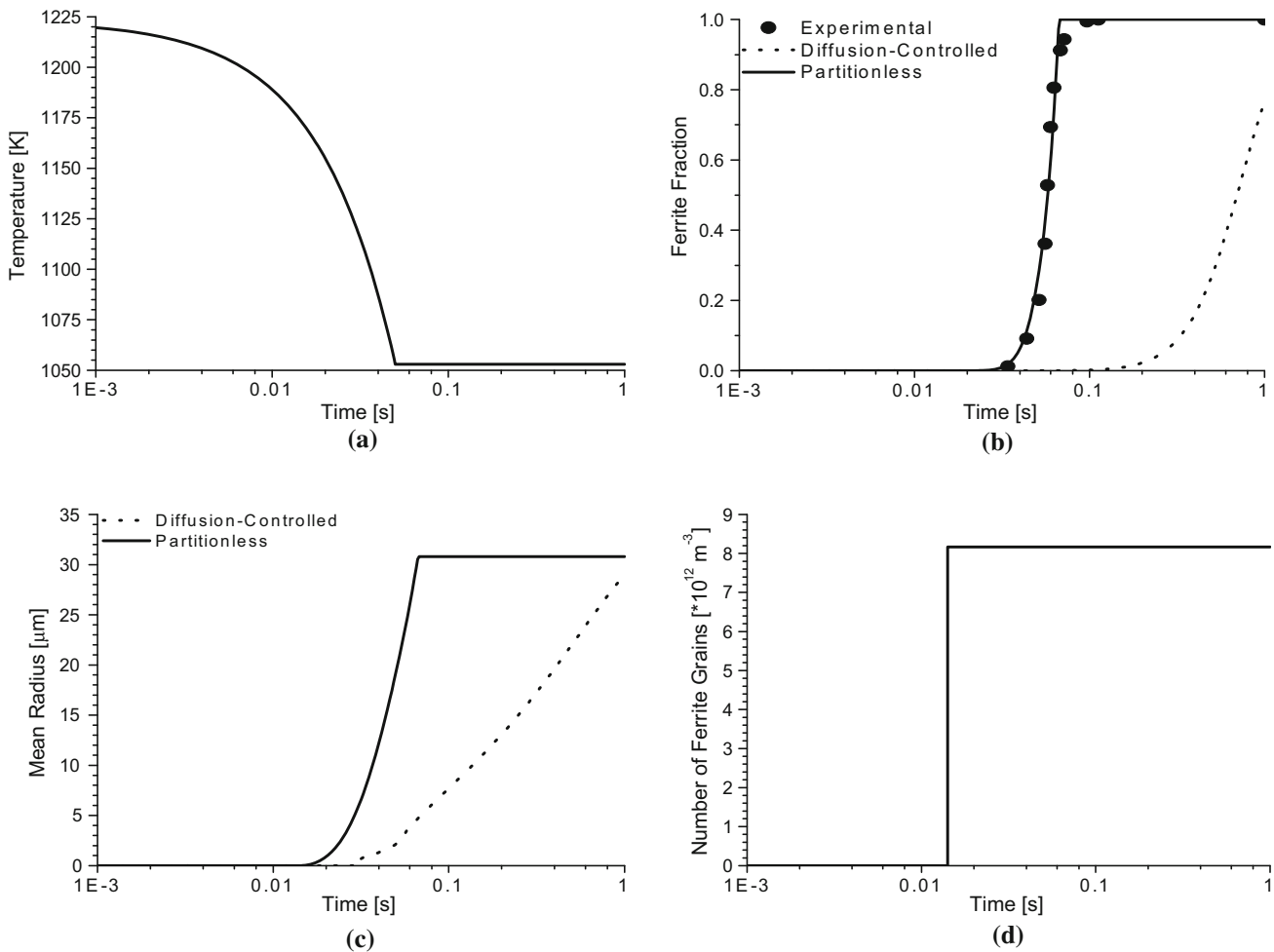


Fig. 13—(a) Cooling curve, (b) ferrite fraction, (c) mean radius, and (d) number of ferrite grains for the hollow sample of alloy A when quenched from 1223 K to 1053 K (950 °C to 780 °C).

In the analysis of heterogeneous nucleation, Clemm and Fisher^[25] showed that nucleation at grain boundary corners can occur instantaneously even without the necessity of overcoming a nucleation barrier by thermal activation. In Figure 13(d), this effect is clearly reflected in the observation that nucleation happens practically instantaneously after crossing the phase boundary. This effect is due to the removal of original grain boundary area by the nuclei of the ferrite phase.

2. Solid samples

In the case of solid samples of alloy A, austenitized at 1223 K to 1373 K (950 °C to 1100 °C), two distinct transformation regimes can be identified (Figures 11(b) and (c)). At 1143 K to 1163 K (870 °C to 890 °C), the evolution of ferrite fraction occurs with slower kinetics, indicating that the transformation involves C partitioning. On the other hand, at IT annealing temperatures from 1053 K to 1133 K (780 °C to 860 °C), the ferrite profile evolution occurs under fast reaction kinetics, suggesting a massive transformation mechanism.

The effect of austenitization temperature on the transformation kinetics is rationalized by comparison of the ferrite evolution profiles for annealing at 1223 K

and 1373 K (950 °C and 1100 °C), particularly at temperatures from 1143 K to 1163 K (870 °C to 890 °C) (Figure 11). Presumably, larger austenite grains, as a consequence of the higher austenitization temperature of 1373 K (1100 °C), lead to slower transformation kinetics due to a reduced number of potential nucleation sites for ferrite at the austenite grain boundaries and larger diffusion distances for C accompanying ferrite growth.

B. Alloy B

Ferrite fraction profiles (Figure 12) of alloy B show relatively slower kinetics in all cases. These profiles indicate that the alloying element (*i.e.*, C) partitions during the transformation process. For validation, calculations performed for PE nucleation and growth conditions are shown in Figure 14. Additionally, partitionless kinetics is also shown in Figure 14 for comparison. Grain corners are assumed to be the most probable nucleation sites. The nucleus composition (para C content) can be assessed from the phase diagram (Figure 9).

In the calculation, a sample of alloy B is quenched from an austenitization temperature of 1223 K (950 °C)

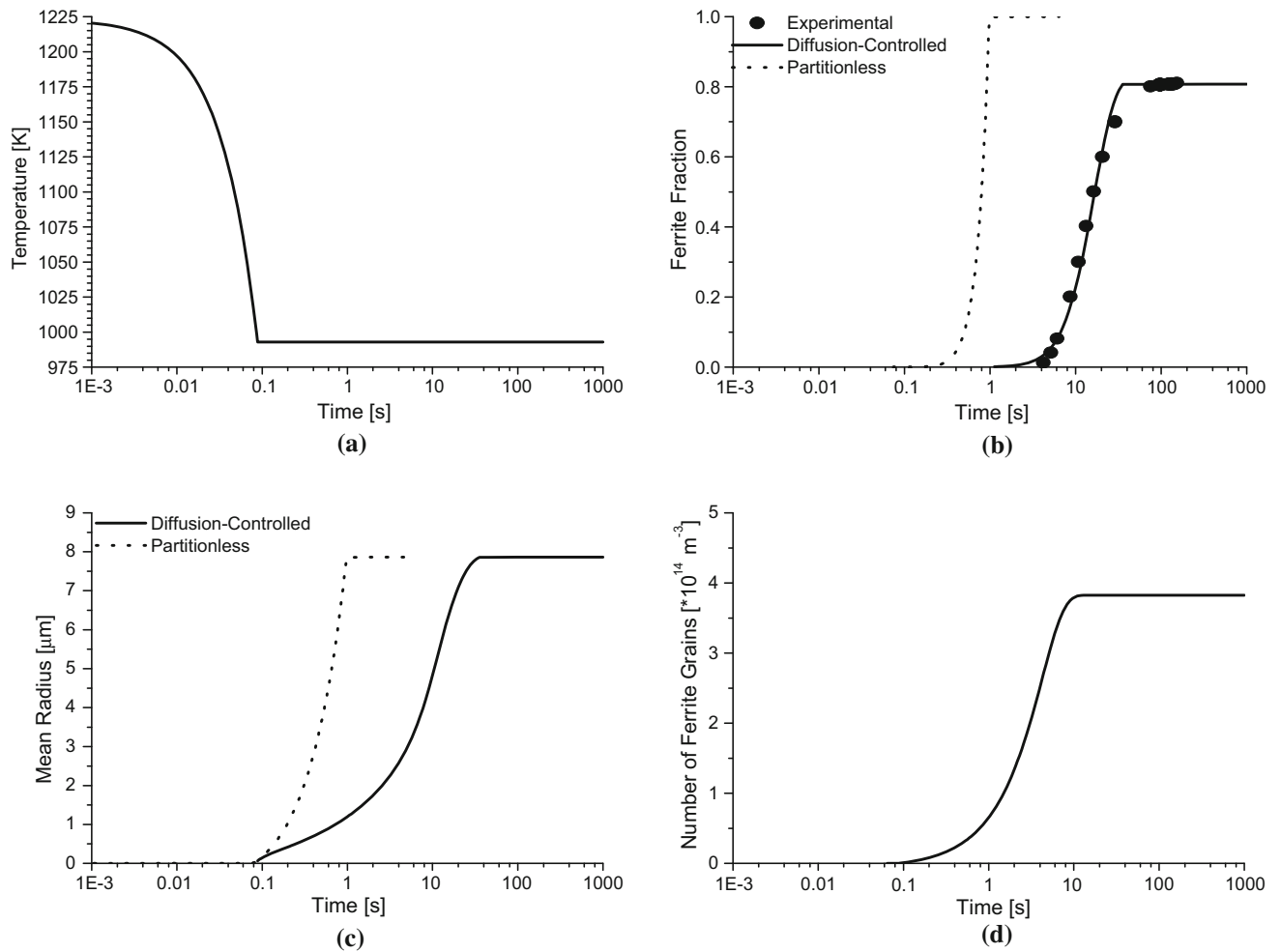


Fig. 14—(a) Cooling curve, (b) ferrite fraction, (c) mean radius, and (d) number of ferrite grains for the hollow sample of alloy B when quenched from 1223 K to 993 K (950 °C to 720 °C).

to the IT annealing temperature of 993 K (720 °C) (Figure 14(a)). Using PE conditions and the assumption of a diffusion-controlled transformation, the MatCalc simulation closely reproduces the experimentally measured transformed ferrite fraction (Figure 14(b)). The measured grain size is 16 μm . The simulated evolution of the half grain size is shown in Figure 14(c). The predicted interfacial energy of 36.2 mJ/m^2 is slightly modified to 29.5 mJ/m^2 to obtain the experimentally observed half grain size after completion of the transformation, which is basically determined by the density of ferrite nuclei.

V. SUMMARY

The IT austenite decomposition kinetics is studied in ULC steel with $w_c = 0.004$ pct C and LC steel with $w_c = 0.11$ pct C using a high-speed quenching dilatometer. Two types of cooling rates, *i.e.*, maximum cooling rates between 900 K/s and 3400 K/s as well as 40 K/s, are used. The highest cooling rates are achieved for hollow cylindrical samples such that the He-jet

simultaneously quenches the internal and external walls of the samples.

In the two-phase α plus γ region, the ULC steel shows a characteristic two-stage transformation, with the transformation starting off in partitionless mode. In the second stage, the transformation kinetics is controlled by long-range diffusion of C. In the single-phase region [*i.e.*, 1053 K to 1133 K (780 °C to 860 °C)], all samples show entirely partitionless growth kinetics in response to cooling rates up to 3400 K/s. The calculated (*i.e.*, 26.5 mJ/m^2) ferrite/austenite interfacial energy for planar sharp interfaces indicates that nucleation is easy and occurs with almost no undercooling. Taking into account the reduction of interface energy due to heterogenous nucleation at the grain boundary edges and corners further facilitates the rapid nucleation, which is observed experimentally.

In the simulations, the pre-exponential factor is taken to be $5 \times 10^{-4} \text{ mol s kg}^{-1} \text{ m}^{-3}$ and the activation energy is 140 kJ mol^{-1} . In the solid samples, the growth kinetics is controlled by partitioning of C in the two-phase γ and α regions. In the single-phase α region, we observe diffusion-controlled growth at higher temperatures. At lower temperatures, these samples show a

two-stage or entirely partitionless massive transformation mechanism.

In comparison, in the LC steel samples, only diffusion-controlled transformation kinetics is observed irrespective of the quenching rate. Calculations indicate that the most probable nucleation sites are grain boundary corners, and only a minor correction of the predicted interfacial energy is required to reproduce the experimentally measured transformed ferrite fraction.

ACKNOWLEDGMENTS

One of the authors (FI) acknowledges the financial support of the Higher Education Commission (HEC), Government of Pakistan.

REFERENCES

1. H.K.D.H. Bhadeshia: *Progr. Mater. Sci.*, 1985, vol. 29, pp. 321–86.
2. J.W. Christian: *Phase Transformations*, York Conference, Institution of Metallurgists, 1979, vol. 1.
3. T.B. Massalski: *Phase Transformations*, ASM, Metals Park, OH, 1970, p. 433.
4. M.J. Bibby and J.G. Parr: *J. Iron Steel Inst.*, 1964, vol. 202, pp. 100–04.
5. E. Kozeschnik and E. Gamsjäger: *Metall. Mater. Trans. A*, 2006, vol. 37A, pp. 1791–97.
6. Y.C. Liu, F. Sommer, and E.J. Mittemeijer: *Acta Mater.*, 2006, vol. 54, pp. 3383–93.
7. Y. Liu, D. Wang, F. Sommer, and E.J. Mittemeijer: *Acta Mater.*, 2008, vol. 56, pp. 3833–42.
8. Z. Barber: *Introduction to Materials Modelling*, Maney Publishing, Leeds, 2005, pp. 73–96.
9. *High-Speed Quenching Dilatometer (805A), Manual*, BÄHR Thermoanalyse GMBH, Hüllhorst, Germany.
10. M. Mehta: *ASTM Specification A 1033-04*, ASTM, West Conshohocken, PA, 2004.
11. J. Svoboda, F.D. Fischer, P. Fratzl, and E. Kozeschnik: *Mater. Sci. Eng. A*, 2004, vol. 385, pp. 166–74.
12. E. Kozeschnik, J. Svoboda, P. Fratzl, and F.D. Fischer: *Mater. Sci. Eng. A*, 2004, vol. 385, pp. 157–65.
13. *MatCalc, Thermodynamic Database "mc_fe_v1.14,"* E. Povoden-Karadeniz, ed., Vienna University of Technology, Vienna, 2014.
14. A. Jablonka, K. Harste, and K. Schwerdtfeger: *Steel Res.*, 1991, vol. 62, pp. 24–33.
15. *MatCalc, Physical Database "PhysData_fe_v1.03,"* E. Povoden-Karadeniz, ed., Vienna University of Technology, Vienna, 2014.
16. A. Van der Ven and L. Delaey: *Progr. Mater. Sci.*, 1996, vol. 40, pp. 181–264.
17. Z.-K. Liu and J. Agren: *Acta Metall.*, 1989, vol. 37, pp. 3157–63.
18. M. Hillert: *Metallurgy Paraequilibrium and Other Restricted Equilibria*, MRS Symp. Proc., Elsevier Science Publishing Co., Inc., Amsterdam, 1983, vol. 19, pp. 295–309.
19. M. Enomoto and H.I. Aaronson: *Scripta Metall.*, 1985, vol. 19, pp. 1–3.
20. E. Kozeschnik: *J. Phase Equilib.*, 2000, vol. 21, pp. 336–47.
21. S.K. Bhattacharyya, J.H. Perepezko, and T.B. Massalski: *Scripta Metall.*, 1973, vol. 7, pp. 485–88.
22. B. Sonderegger and E. Kozeschnik: *Metall. Mater. Trans. A*, 2009, vol. 40A, pp. 499–510.
23. B. Sonderegger and E. Kozeschnik: *Scripta Mater.*, 2009, vol. 60, pp. 635–38.
24. B. Sonderegger and E. Kozeschnik: *Metal. Mater. Trans. A*, 2010, vol. 41A, pp. 3262–69.
25. P.J. Clemm and J.C. Fisher: *Acta Metall.*, 1955, vol. 3, pp. 70–73.
26. W.S. Rasband: *ImageJ*, U.S. National Institutes of Health, Bethesda, MD, <http://rsb.info.nih.gov/ij/>, 1997–2009.
27. K.G.F. Janssens, D. Raabe, E. Kozeschnik, M.A. Miodownik, and B. Nestler: *Computational Materials Engineering: An Introduction to Microstructure Evolution*, 1st ed., Elsevier Academic Press, Cambridge, 2007.
28. *MatCalc, Diffusion Database "mc_fe_v1.03,"* E. Povoden-Karadeniz, ed., Vienna University of Technology, Vienna, 2014.
29. M. Hillert: *Metall. Trans. A*, 1975, vol. 6A, pp. 5–19.
30. G.P. Krielaart and S. van der Zwaag: *Mater. Sci. Technol.*, 1998, vol. 14, pp. 10–18.